Insights on the clay reactivity in alkaline media: Beyond filler role for kaolin

Emilie Emmanuel, Mickaël Paris, Dimitri Deneele

Insights on the clay reactivity in alkaline media: beyond filler role for kaolin

Emilie Emmanuel[a], Michael Paris[a,*], Dimitri Deneele[a,b,*]

[a] Institut des Matériaux Jean Rouxel (IMN), Université de Nantes, CNRS, 2 rue de la Houssinière, BP 32229, 44322 Nantes Cedex 3, France

[b] IFSTTAR, GERS, EE, F-44344 Bouguenais, France.

*Corresponding authors

Phone : + 33 2 40 84 58 02 (DD) / + 33 2 40 37 39 01 (MP)

Fax: + 33 2 40 58 57 77 (DD) / + 33 2 40 37 39 95 (MP)

Abstract:

Beside lime and hydraulic binders, alkaline activation recently emerges as a possible solution for soil stabilization. Unfortunately, soil reinforcement by alkaline activation requires additional reactive aluminosilicate sources under ambient temperature. In this study, we focus on kaolin as a simplified model of kaolin-rich soils which show limited improvement on mechanical performance after lime treatment. Here, we explore the reactivity of kaolin after a two-step process combining NaOH activation and sodium silicate solution activation. We show that kaolin reactivity is greatly enhanced compared to sodium silicate solution activation only. After the two-step process, the formed phases differ depending on the setup of the NaOH activation. More interestingly, for well chosen conditions, a large amount of highly depolymerized gel is created, which is expected to improve the mechanical performance of treated kaolin clay soils.

Keywords: Kaolin, alkaline activation, NaOH, Zeolite, depolymerized gel

1. Introduction

The alkali-activated materials with the development of geopolymers and so on, from the alkaline activation of calcined clays or industrial by-products is today well-developed (Provis et al., 2018). Kaolin alkaline activation is probably the best mean to get a geopolymer developing excellent properties and ensuring very good durability. Obviously, the improvement of the kaolin reactivity goes through the thermal activation giving the dehydroxylated kaolin, the metakaolin. The use of calcined clays in the development of original binders is more and more developed since the latest generation of alkaline cements are multi-component system, consisting in blends with high mineral addition and low cement content (Garcia-Lodeiro et al., 2018).

If the use of dehydroxylated kaolinite is now common in the alkali-activated materials, MacKenzie et al., (2007) studied the possibility to produce viable inorganic polymers without the need to dehydroxylate the solid aluminosilicate. Theirs results indicate that under standard geopolymer synthesis conditions, an undehydroxylated clay will not achieve the full strength and texture of a well-cured geopolymer. The material is of poor crystallinity and is consistent with a partially-formed geopolymer. Afterwards, as an alternative to thermal dehydroxylation, high-energy grinding of the solid phase (the clay mineral) was tried. The ground product proved to be a much more satisfactory starting material, hardening to forming a product with signature of typical geopolymer. However, energy still has to be supplied to the system by grinding, so chemical pretreatment of the solid reactant with acid or alkali was also investigated. However, treatment of the clay with HCl gave the same result as the raw clay, namely, a poorly-formed geopolymer. On the other hand, treatment of the clay with sodium hydroxide produced a hydrated zeolite and again, converted a significant amount of the

50 Al(VI). The geopolymer formed from this material hardens and mainly contains Al(IV), and a
51 crystalline sodium aluminium carbonate.
52 In fact, geopolymers are often described as amorphous materials, almost identical to some
53 silicate gels (Brinker et Scherer, 1990) and aluminosilicate zeolite gel precursors prior to
54 crystallization. Hydrothermal alkaline reaction of kaolin clay, metakaolin, fly ashes, and some
55 different aluminosilicate materials result in the formation of zeolites with various frameworks
56 depending on the reaction conditions (temperature, alkali cation, Si/Al ratio etc.). The
57 exploration of new ways of zeolitization are today explored since concerns about energy
58 consumption, carbon economy and production costs have called the attention of researchers to
59 seek for cheaper raw materials for its synthesis in place of using pure synthetic starting raw
60 materials (Ayele et al., 2016).
61 At the same time, the alkaline activation of clay minerals at low temperature could be
62 considered for soil stabilisation. Provis and Van Deventer (2014) have mentioned the ability
63 to utilise local naturally occurring raw materials (pozzolanic soils and clays) as AAM
64 precursors will be highly desirable in regions lacking in hydraulic binders. Besides, each
65 family of minerals reacts differently under alkaline condition. Except the study of Verdolotti
66 et al (2008) who explored whether the geopolymerization could be adopted as a methodology
67 to consolidate incoherent pozzolana soils, any known studies on the use of alkali activated
68 materials for soil stabilisation required the use of an additional reactive aluminosilicate source
69 under ambient temperature. The study of Verdolotti et al. (2008) is very particular since *in*
70 *situ* alkali activation of pozzolanic soils gives a strong material.
71 Other works on alkali activated soil are recent and aim to stabilise different types of soil from
72 clayey soil (Wilkinson et al., 2010; Singhi et al., 2016), sandy clay (Cristelo et al., 2011),
73 marl, marlstone (Cristelo et al., 2012), silty sand (Rios et al., 2016), road aggregates (Tenn et
74 al., 2015) to mixed soil synthesised in laboratory (Sargent et al., 2013; Zhang et al., 2013).

In each cases, an aluminosilicate material was used. The overall works showed the potential of alkaline activation for soil improvement and this for different designed applications. Cristelo et al., (2011), for instance, demonstrated that alkaline activation is a viable technique to be applied in deep soft soil improvement, more specifically to jet grouting columns. While Zhang et al. (2013) described a different potential application of alkali activated soil stabilisation at shallow depth (i.e. subgrade, sub-base, shallow foundation, embankment etc.). Or else, Silva et al. (2013) proved the use of alkaline activation of fly ash as a stabilisation technique to be capable of improving the performance of rammed earth construction.

The understanding of the soil reactivity as a whole faced to alkaline activation could be complicated and ambitious since it exists several limiting factors affecting the geopolymerisation process. For instance, the complexity of soils which contains various mineral phases of different particle size, shape and composition renders difficult to predict soil behaviour following alkaline attack. Recently, Marsh et al. (2019) highlighted a lack of understanding of how soil composition influences the alkali activation reaction and mentioned Montmorillonite seems to be more reactive than kaolinite, but kaolinite has a stronger influence in determining reaction products. Before to think about the soil stabilisation by alkaline activation, we propose here to study a simplified soil consisting of a single clay mineral. Among all clay minerals, we have chosen a kaolin since kaolin-rich soils are often problematic in stabilization processing. This paper is an attempt to get a better understanding of the effect of the chemical activation of kaolin in alkaline medium at low temperature. It describes a two-step process combining NaOH activation and sodium silicate solution activation which greatly enhances kaolin reactivity. The evolution of reaction products was followed using X–Ray diffraction (XRD), solid-state Nuclear Magnetic Resonance (NMR) and Scanning Electron Microscopy (SEM).

2. Materials and experimental methods

2.1 Materials

The kaolin used in that study is the kaolin speswhite from Imerys Company. It is composed of 95 wt.% of kaolinite, 4 wt.% of muscovite. The rest are Quartz and goethite traces (Chemeda et al. 2015). Particle sizes are between 10 and 0.2 μm with a D50 of 0.7 μm. Pretreatment solutions are aqueous solutions of NaOH at concentrations of 5M and 10M. Industrial solution of sodium silicate (Geosil® No. 34417) was provided by Wöllner. Weight ratio SiO2/Na2O is 1.70 and solid content is 44%.

2.2 Sample preparation

Alkaline activation was done by mixing raw kaolin with Geosil solution, giving the following ratio respectively: Si/Al=1.8, Si/Na=1.7 and Al/Na=1. After manual shacking, the closed reactor was stored in an oven at 40°C. At each curing time (7and 90 days), samples were freeze-dried before analyses.

NaOH pre-activation was realized with NaOH solution at 5 and 10 M in closed reactors, at room temperature. 3 different curing time were tested 1, 3 and 7 days. At the end of this phase, the Geosil solution was added giving the final ratio for 5M and 10M respectively: Si/Al=1.77, Si/Na=1.25, Al/Na=0.71 and Si/Al=1.77, Si/Na=1 and Al/Na=0.56. The closed reactors were stored in an oven at 40°C and samples were freeze-dried before analyses.

Sample preparation consisted in (i) mix of the Raw speswhite kaolin (Kraw) with Geosil alkaline solution named Kxd with x the curing time in days (ii) Raw speswhite kaolin with a yM NaOH solution for x days (KyMxd) with y= 5M or 10M (iii) alkali activated kaolin at 90 days of curing with prior chemical pretreatment of x days at yM NaOH and named KyMxd_90d. Figure 1 gives a sketch of the synthesis conditions.

2.2 X-ray diffraction analysis

X-ray diffraction was performed using Bruker D8 Advance powder diffractometer, which operates in Bragg-Brentano geometry with a Cu anode sealed x-ray tube (Cu Kα1 radiation; λ = 1.540598 Å) and a focusing Ge (111) primary monochromator. The X-ray tube was operated at a voltage of 40 kV and a current of 40 mA. The scanning was performed over angular range 2θ from 5° to 60° and a step size of 0.018°.

2.3 Nuclear Magnetic Resonance

^{29}Si solid state MAS (Magic Angle Spinning) NMR spectra were acquired on a 300 MHz Bruker Avance III using a 7 mm MAS probe. The ^{29}Si MAS NMR spectra were acquired with a single π/2 pulse excitation of 5.5 μs and recycle time of 60 s. For ^{1}H- ^{29}Si Cross-Polarization (CP) spectra, the contact time was set to 0.5 ms. MAS frequency was set to 30 kHz and the recycle delay between scans to 60 s and 1s for direct and CP acquisitions, respectively.

^{1}H and ^{27}Al MAS NMR spectra were acquired on a 500 MHz Bruker Avance III using a 2.5 mm MAS probe. The MAS frequency was set to 30 kHz and the recycle delay to 1s. The ^{1}H MAS NMR spectra were using a Hahn echo (π/2 - τ - π - τ - acq) acquisition with a π/2 pulse of 3.5 μs et τ equal to one MAS period. The ^{27}Al MAS NMR spectra were acquired with single π/13 excitation for a radiofrequency strength (r.f.) strength of 11 kHz.

For all ^{29}Si and ^{27}Al acquisitions, SPINAL64 ^{1}H decoupling scheme was used during acquisition with a r.f. strength of 60 kHz. Spectra were referenced against TMS (Tetramethylsilane) for ^{29}Si and ^{1}H and against $Al(NO_3)_3$ in aqueous solution for ^{27}Al.

149 2.4 Scanning electron microscopy

150 Microstructural and morphological features of samples have been observed through Scanning
151 Electron Microscopy (SEM) by using Hitachi SU5000 microscope. A gold coating has been
152 performed on dehydrated samples before SEM observations.

153

154 3. Results and discussion

155

156 3.1 Alkali activation of the raw kaolin

157

158 After curing, XRD diagrams (Figure S1) only show the formation of Thermonatrite after 7
159 days of curing as new secondary crystalline compound. There is a decrease of the Muscovite
160 content whereas the patterns of Kaolinite in K7d and K90d are almost identical to the one of
161 the raw Kaolinite.

162 Figure 2 shows the ^{29}Si and ^{27}Al MAS NMR spectra of Kraw, K7d and K90d. ^{29}Si NMR
163 signals of Kaolinite and Muscovite appear at -91 and -85 ppm, respectively. The ^{27}Al signal
164 between -10 and 30 ppm comes from the octahedral sheets of both Kaolinite and Muscovite
165 whereas the 70 ppm line originates from aluminium within the tetrahedral sheets of
166 Muscovite. After Geosil activation, a new line at ~60 ppm, associated with aluminium in
167 tetrahedral environment, appears in the ^{27}Al spectrum. As kaolin is the only source of
168 aluminium, the weak intensity of this line shows the low reactivity (i.e. low dissolution) of
169 kaolin to Geosil activation in agreement with XRD observation.

170 The ^{29}Si spectrum of K7d shows a shoulder at ~-94 ppm and two well-defined signals at -86
171 and -78 ppm associated with Q_3, Q_2 and Q_1 moieties, respectively. This suggests the presence
172 of a gel phase (hereafter referred as gel1) made of chains and/or small oligomers as those
173 observed in the Na-silicate solution (Duxson et al., 2005; Harris et al., 1995).

After a curing time of 90 days, gel1 has turned into a new gel phase (gel2) characterized by two broad signals at ~ -84 and ~ -76 ppm corresponding to larger distributions of Q_2 and Q_1 environments than in K7d. Q_1/Q_2 was estimated at ~1.2 for gel2 and $Q_1/(Q_2+Q_3)$ at ~0.2 for ge1 1. Therefore, gel2 turns out to be more depolymerised than gel1.

In addition to the hydroxyl signals of the raw Kaolinite at 1.9 and 2.8 ppm, the ^1H spectra exhibit a strong signal at 6.1 ppm for K7d and a weak and broader signal at 6.4 ppm for K90d (Figure S2). Both signals are attributed to hydroxyls or molecular water embedded in gel1 and gel2. These two different ^1H signatures support the structural evolution of the gel during curing and suggest that higher ^1H chemical shift is associated with more depolymerised gel structure.

In contrast with gel2, gel1 is not observed by $^1H/^{29}Si$ CPMAS (Cross-Polarization and Magic Angle spinning) approach with short contact time (Figure 2). The lack of $^1H/^{29}Si$ CP signal for gel1 is likely due to higher mobility of constituting species since gel1 incorporates more water than K90d as shown by the ^1H MAS spectra (Figure S2). The mobility of constituting species, in contrast, appears to be limited in gel2. Reduced water content and mobility suggest that the gel get denser with time.

This conclusion is further supported by SEM observations which reveal, after the Geosil addition, the presence of the gel phase covering the Kaolinite particles (Figure 3). This gel fits closely the initial particles of Kaolinite. The increase of the curing time shows a denser gel but no clear modification can be detected about the gel depolymerisation.

3.2 NaOH activation of kaolin

XRD diagrams (Figure S3) of 5M NaOH activated compounds reveal the presence of

199 Hydrosodalite (HS) and carbonates with increasing curing time. HS is only visible at 3 days.
200 The formation of Thermonatrite at 1 day is later completed by the appearance of Natrite at 7
201 days of curing. For 10M NaOH, HS occurs at the same time step (3 days) and then decreases
202 but is still detected at 7 days. Kaolinite seems stable over time and the Muscovite content
203 decreases.
204 Besides Kaolinite signals, only the ^{27}Al (63 ppm) and ^{29}Si (-86 ppm) additional lines are
205 observed in the ^{29}Si and ^{27}Al NMR spectra of K5Mxd and K10Mxd for x=1, 3 and 7 (Figure
206 4). According to Madani et al (1990), they are attributed to HS in full agreement with the only
207 new phase detected by XRD (Figure S3) and visible by SEM (Figure 5).
208 However, although the variation of the amount of HS detected by ^{29}Si NMR agrees with XRD
209 for the K10Mxd series (i.e. no HS detected at 1d and decrease after 3d), it slightly differs for
210 the K5Mxd series. Indeed, in contrast with XRD, the presence of HS is clearly detected by
211 NMR as soon as 1d. Also, the variations of HS amount from 1d to 3d detected by XRD and
212 NMR disagree since there is no difference in the HS proportion from the ^{29}Si NMR point of
213 view. The signal at 5.0 ppm in the ^{1}H MAS NMR spectra of 5M NaOH activated samples
214 (Figure S4) is attributed to water in the sodalite cages of HS (Buhl et al., 1988). Its intensity
215 change fully supports the observed variations of HS by ^{29}Si NMR through the -86 ppm line.
216 The discrepancies between XRD and NMR in HS amount can be explained by the poor
217 quality and the small sizes of the HS crystallites formed under ambient temperature. Finally,
218 the ^{1}H spectra of K10M1d and K10M7d (Figure S4) also show a line at 5.5 ppm which is
219 assigned to hydroxyls or water molecules of the depolymerized component associated with
220 the broad ^{29}Si signal observed between -70 and -83 ppm.
221 SEM was performed to further investigate the phase relationships (Figure 5). For both NaOH
222 concentrations, SEM examination shows the degradation of Kaolinite platelets exhibiting an
223 external shape partially cut and coated. The platelets are covered by the gel phase. The

formation of new phases from the gel is obvious at 1 day, developing on both the basal faces and edges of the platelets. The increase of the NaOH content leads to the increase of the Kaolinite dissolution and in turn to an increase of the secondary phase formation. These precipitates correspond to Hydrosodalite phase as detected by XRD and described by NMR. Increasing the curing time, we observe an in-situ partial carbonation of HS, confirming the detection of Thermonatrite by XRD (Figure S3).

3.3 Geosil activation of kaolin with prior NaOH activation

In the two previous sections, we have proved that, in our experimental conditions, raw kaolin hardly reacts with sodium silicate solution but reacts with sodium hydroxide solution to form HS. In this section, we will show that these two reactivity schemes can interact together and cause the system to explore new routes.

Let us first describe the Geosil activation of kaolins with prior NaOH activation at 10M NaOH. XRD analysis of K10M1d_90d and K10M7d_90d samples (Figure S5) only reveal the formation of HS, similarly to the evolution of the system during the NaOH activation. In addition, in both samples, we note the formation of Natrite. SEM observations (Figure 6) are also similar to those did after NaOH activation. A gel on which we can observe the formation of secondary compounds, here HS, develops at the surface of the Kaolinite platelets. We note an average decrease of the mean porosity or a densification of the samples by a spreading of the gel leading to better connectivity between Kaolinite platelets.

In contrast with XRD, ^{29}Si NMR results -exhibit strong differences between K10M1d (Figure 4) and K10M1d_90d (Figure 7) samples as well as between K10M7d (Figure 4) and K10M7d_90d (Figure 7). For K10M7d_90d, the presence of HS fits adequately the final state of NaOH activation and the broad ^{29}Si lines at -84 and -76 ppm resemble the signature of gel2

observed in K90d (Figure 2). This interpretation is further supported by the presence of the broad and weak line at 6.4 ppm in the ^{1}H spectrum of K10M7d_90d (Figure S6). For K10M1d_90d, both ^{29}Si and ^{27}Al spectra (Figure 7) show the presence of a significant proportion of HS, yet totally absent before sodium silicate addition. Moreover, the ^{29}Si NMR lines at -94, -84 and -78 ppm resemble the signature of gel1 observed in K7d (Figure 2). A slightly variant interpretation of the spectrum would attribute the signal at -84 ppm in the ^{29}Si spectrum of K10M1d_90d to gel2 and the signal at -86 ppm to both HS and gel1. This interpretation better agrees with the chemical shifts observed for gel1 in K7d (-86 ppm rather than -84 ppm) and with the similar line widths of the signals at -78 and -86 ppm. Moreover, the detection of the -84 ppm line by the $^{1}H/^{29}Si$ CP approach (Figure 7) confirms its attribution to gel2 while the contribution of gel1 (and HS) at -94, -86 and -78 ppm are totally absent as in K7d. In any case, the presence of gel1 is unambiguously proved by the strong 6.0 ppm line in the ^{1}H spectra of K10M1d_90d (Figure S6). Hence, the growth of HS during the curing of K10M1d_90d seems to hinder or slow down the transformation of gel1 to gel2 (observed for direct Geosil activation) while for K10M7d_90d, HS formed during prior NaOH activation does not play any role in the gel evolution.

We have just seen that the alkali activation of 10M NaOH treated kaolin is actually a mix of the reaction occurring during the two stages. Although NaOH activations at 5M and 10M seems to act similarly, the subsequent behavior under alkali activation by sodium silicate after NaOH activation at 5M strongly differs from the one at 10M just described above.

After 1 day of NaOH activation at 5M, XRD diagram (Figure S5) shows the formation of Faujasite, while an increase of the time of NaOH activation (7 days) leads to the formation of Phillipsite rather than Faujasite. Natrite is also detected in addition to Phillipsite. The microstructure of the synthesized materials is similar to those observed above. The sample is mainly composed of a gel covering the kaolin particles; we note the development of

secondary phases at the expense of the gel, Faujasite and Phillipsite, after 1 day and 7 days of 5M NaOH pre-activation, respectively.

Figure 7 shows the ^{27}Al and ^{29}Si NMR spectra of K5M7d_90d. The ^{29}Si lines at -108,-102,-97 and -87 ppm are attributed to the Q_4(0Al), Q_4(1Al), Q_4(2Al) and Q_4(4Al) units of Phillipsite as well as the ^{27}Al signal at 60 ppm(Madani et al., 1990; Ciccioli et al., 2010). Although, the ^{29}Si lines at -84 and -78 ppm look like the gel2 signature, they are hardly visible in the ^{1}H/^{29}Si CP spectrum (Figure 7) and the ^{1}H signal is strong rather than weak and broad (Figure S6). Therefore, this gel seems to be in between gel1 and gel2, i.e. the local structure of gel2 with the mobility of gel1.

For Na-X zeolite with low Si/Al of 1.18, the ^{29}Si signal of highest intensity was reported at -85 ppm (Lippmaa et al., 1981). All other signals appear at lower chemical shifts. As no HS is detected by XRD (Figure S5), as the signal for Al(IV) appears at 59 ppm (Figure 7) rather than 63 ppm (HS) and as no ^{1}H signal is visible at 5.0 ppm (Figure S6), we attribute the ^{29}Si signal of K5M1d_90d at -86 ppm to Na-X zeolite (Figure 7). The strong and featureless ^{29}Si signal in the -70 to -85 ppm range exhibits a much more intense contribution of the Q_1 region (-75 to -80 ppm) than previously observed for gel1 or gel2. This new gel phase (gel3) is easily detectable by ^{1}H/^{29}Si CP (Figure 7) and presents a broad and weak signal ^{1}H at 6.5 ppm (Figure S6). Thus, gel3 is more depolymerized than gel2 and gel1 and is associated with ^{1}H signal of higher chemical shift in accordance with the trend observed for gel1 and gel2.

Concluding remarks:

For all synthesis conditions (Geosil or NaOH activations and their combination), SEM shows that the kaolin particles are covered by a gel. Three type of gel were identified by NMR

299 spectroscopy. Their structures differ and depend on synthesis set-up. For Geosil activation, we
300 only observed the evolution from the early formed gel1 to gel2 after 90 days. In contrast, for
301 NaOH activation, the gel covering the kaolin particles quickly turns to HS after few days.
302 When strong NaOH activation (10M) is carried out before Geosil activation, the formed HS
303 does not react to the Geosil addition. Thus, gel1 is formed and evolves to gel2 under the weak
304 influence of the HS presence. Then, the two activation processes occur independently.
305 For mild NaOH activation (5M) prior to Geosil activation, no more HS is detected and
306 Faujasite and Phillipsite are formed from the covering gel. These two zeolites have a Si/Al
307 ratio greater than 1. This unambiguously proves that the two activation processes are not
308 independent anymore and take place in an unique reactivity scheme. Thus, the benefit of
309 NaOH pre-activation is to promote the reactivity of the kaolin to the Geosil activation as done
310 by the thermal activation of kaolin in the synthesis of geopolymer based on metakaolin.
311 However, the reactivity scheme developed here cannot compete with metakaolin-based
312 geopolymer neither in terms of reactivity level nor usability.
313 Nevertheless, it could be used at profit by the construction industry which often faces the poor
314 mechanical performance of kaolin clay soil in construction sites. For these soils, the usual
315 stabilisers (lime or Ordinary Portland Cement) have shown limited improvement on
316 mechanical performance.
317 Moreover, their production is associated with high CO2 emission. Thus, new approaches for
318 soil stabilisation, which use the alkaline activation of industrial by-products like fly ashes
319 (Coudert et al., 2018) or slags (Wilkinson et al., 2010), have been developed. However, the
320 cost and the availability of such by-products could limit their widespread use.
321 In the present work, we showed that NaOH pre-activation of kaolin in well chosen conditions
322 can improve the reactivity of kaolin to Geosil activation. If so, it is likely that the amount of
323 by-products needed for kaolin clay soil stabilisation can be reduced because kaolin will no

longer act as filler only. In this case, the most useful phase of our process would be the highly depolymerized gel phase (gel3) rather than zeolites. Work under development in our laboratory shows that well chosen conditions can totally inhibit the zeolite formation resulting in a higher quantity of gel phase formed.

Acknowledgments

The authors thank Region Pays de la Loire and FEDER for the NMR spectrometer upgrade (Program PO FEDER-FSE Pays de la Loire, "Jouvence de consoles électroniques de spectromètre de résonance magnétique nucléaire à l'état solide")

References

Ayele L., Pérez-Pariente J., Chebude Y., Díaz I., 2016. Conventional versus alkali fusion synthesis of zeolite A from low grade kaolin, Appl. Clay Sci., 132–133, 485–490.

Brinker, C. and Scherer, G. 1990. The Physics And Chemistry of Sol Gel Processing, Sol Gel Science, Brinker, C. and Scherer, G.Eds, Academic Press, 462p

Buhl, J.-C.; Engelhardt, G.; Felsche, J.; Luger, S.; Foerster, H., 1988. 23Na MAS-NMR and 1H MAS-NMR Studies in the Hydro-Sodalite System. Berichte der Bunsengesellschaft für physikalische Chemie, 92 (2), 176–181.

Chemeda Y., Deneele D., Ouvrard G. 2015. Short-term lime solution-kaolinite interfacial chemistry and its effect on long-term pozzolanic activity, Applied Clay Science, 161, pp.419-426.

Ciccioli, P.; Plescia, P.; Capitani, D., 2010. 1H, 29Si, and 27Al MAS NMR as a Tool to Characterize Volcanic Tuffs and Assess Their Suitability for Industrial Applications. J. Phys. Chem. C, 114 (20), 9328–9343.

Coudert E., Paris M., Deneele D., Russo G. Tarantino A., 2018. Use of alkali activated high-calcium fly ash binder for kaolin clay soil stabilisation: Physicochemical evolution, Construction and Building Materials, 201, pp.539-552.

Cristelo, N., Glendinning, S., Teixeira Pinto, A., 2011. Deep soft soil improvement by alkaline activation. Proc. Inst. Civ. Eng. - Ground Improv., 164, 73–82.

Cristelo, N., Glendinning, S., Fernandes, L., Pinto, A.T., 2012. Effect of calcium content on soil stabilisation with alkaline activation. Constr. Build. Mater., 29, 167–174

Duxson, P.; Provis, J. L.; Lukey, G. C.; Mallicoat, S. W.; Kriven, W. M.; van Deventer, J. S. J. 2005. Understanding the Relationship between Geopolymer Composition, Microstructure and Mechanical Properties. Colloids and Surfaces A: Physicochemical and Engineering Aspects, 269 (1–3), 47–58.

Fernandez-Jimenez A, Palomo A, Criado M., 2005. Microstructure development of alkali-activated fly ash cement: a descriptive model, Cem Conc Res 35, 6, 1204-1209.

Fernández-Jiménez, A., Vallepu, R., Terai, T., Palomo, A., Ikeda, K., 2006. Synthesis and thermal behavior of different aluminosilicate gels. J. Non-Cryst. Solids, 352 , 2061–2066

Garcia-Lodeiro I., Boudissa N., Fernandez-Jimenez A., Palomo A., 2018. Use of clays in alkaline hybrid cement preparation. The role of bentonites, Materials Letters 233, 134–137

Harris, R. K.; Bahlmann, E. K. F.; Metcalfe, K.; Smith, E. G., 1993. Quantitative Silicon-29 NMR Investigations of Highly Concentrated High-Ratio Sodium Silicate Solutions. Magn. Reson. Chem., 31 (8), 743–747.

Johnson, E.B.G., Arshad, S.E., 2014. Hydrothermally synthesized zeolites based on kaolinite: a review. Appl. Clay Sci. 97–98, 215–221.

Lippmaa, E.; Maegi, M.; Samoson, A.; Tarmak, M.; Engelhardt, G., 1981. Investigation of the Structure of Zeolites by Solid-State High-Resolution Silicon-29 NMR Spectroscopy. J. Am. Chem. Soc., 103 (17), 4992–4996.

MacKenzie K. J. D., Brew D R. M., Fletcher R. A., Vagana R., 2007. Formation of aluminosilicate geopolymers from 1:1 layer-lattice minerals pre-treated by various methods: a comparative study, J Mater Sci,42:4667–4674

Madani, A., Aznar, A., Sanz, J., Serratosa, J. M. 1990. Silicon-29 and Aluminum-27 NMR Study of Zeolite Formation from Alkali-Leached Kaolinites: Influence of Thermal Preactivation. J. Phys. Chem., 94 (2), 760–765.

Marsh, A., Heath, A., Patureau, P., Evernden, M., Walker, P. 2019. Phase formation behavior in alkali activation of clay mixtures. Appl. Clay Sci. 175, 10–21.

Provis J. L., 2018. Alkali-activated materials, Cement and Concrete Research 114, 40–48

Provis, J.L., van Deventer, J.S.J., 2014. Alkali Activated Materials, RILEM State-of-the-Art Reports. Springer Netherlands, Dordrecht. 388p.

Provis, J.L., Lukey, G.C., van Deventer, J.S.J., 2005. Do geopolymers actually contain nanocrystalline zeolites? – A reexamination of existing results. Chem. Mater. 17 (12), 3075–3085

Rios, S., Cristelo, N., Viana da Fonseca, A., Ferreira, C., 2016. Structural Performance of Alkali-Activated Soil Ash versus Soil Cement. J. Mater. Civ. Eng., 28, 4015125.

Sargent, P., Hughes, P.N., Rouainia, M., White, M.L., 2013. The use of alkali activated waste binders in enhancing the mechanical properties and durability of soft alluvial soils. Eng. Geol., 152, 96–108.

Silva, R.A., Oliveira, D.V., Miranda, T., Cristelo, N., Escobar, M.C., Soares, E., 2013. Rammed earth construction with granitic residual soils: The case study of northern Portugal. Constr. Build. Mater.,47, 181–191.

Singhi, B., Laskar, A.I., Ahmed, M.A., 2016. Investigation on Soil–Geopolymer with Slag, Fly Ash and Their Blending. Arab. J. Sci. Eng., 2016, 41, 393–400

Tenn, N., Allou, F., Petit, C., Absi, J., Rossignol, S., 2015. Formulation of new materials

399 based on geopolymer binders and different road aggregates. Ceram. Int., 2015, 41, 5812–
400 5820.
401 Van Deventer J.S.J., Provis J.L., Duxson P., Lukey G.C., 2007. Reaction mechanisms in the
402 geopolymeric conversion of inorganic waste to useful products, Journal of Hazardous
403 Materials, 139, 3, 506-513
404 Verdolotti, L., Iannace, S., Lavorgna, M., Lamanna, R., 2008. Geopolymerization reaction to
405 consolidate incoherent pozzolanic soil. J. Mater. Sci., 43, 865–873.
406 Wilkinson, A., Haque, A., Kodikara, J., 2010. Stabilisation of clayey soils with industrial by-
407 products: part A. Proc. Inst. Civ. Eng. - Ground Improv. 163,149–163.
408 Zhang, M., Guo, H., El-Korchi, T., Zhang, G., Tao, M., Experimental feasibility study of
409 geopolymer as the next-generation soil stabilizer. Constr. Build. Mater., 2013, 47, 1468–
410 1478

Figure 1 (Emmanuel et al.)

Sketch of the synthesis conditions and labeling of samples

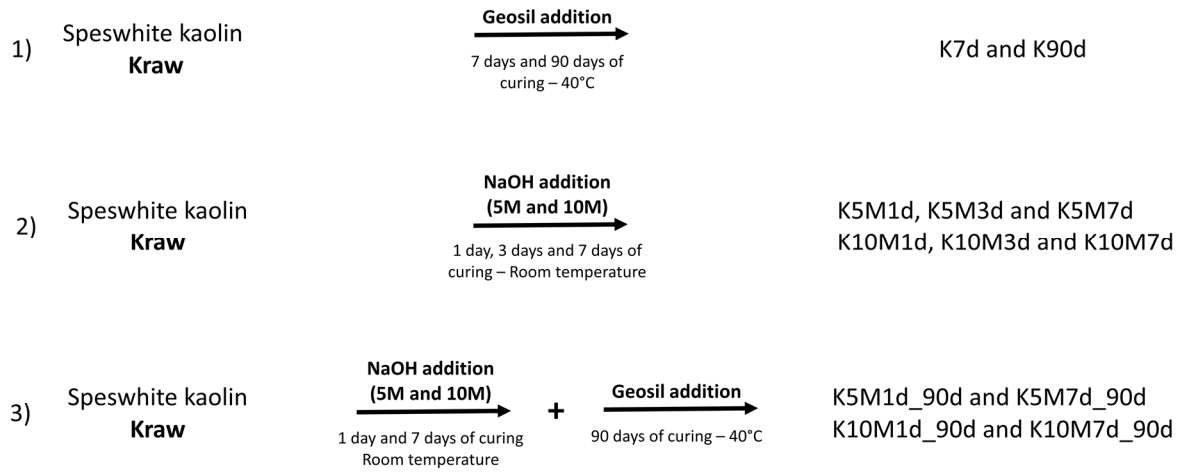

Figure 2 (Emmanuel et al.)

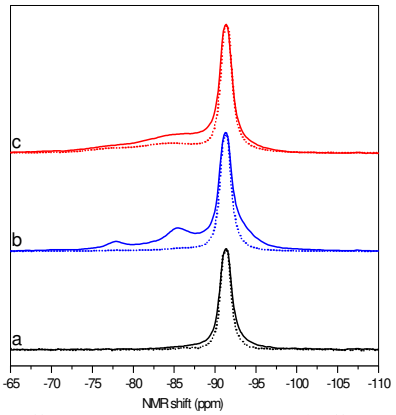

A- ^{29}Si MAS (straight lines) and ^{1}H-^{29}Si CP-MAS (dot lines) spectra of Kraw (a), K7d (b) and K90d (c). MAS spectra of K7d and K90d are normalized to the same area. CP-MAS are normalized to the kaolinite signal (-91 ppm) used as an internal reference to highlight the difference of CP efficiency in the new phases formed.

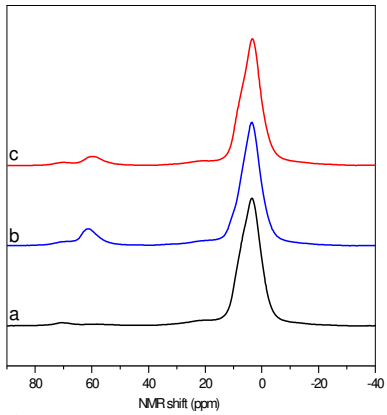

B- ^{27}Al MAS spectra of Kraw (a), K7d (b) and K90d (c). Spectra are normalized to the same area.

Figure 3 (Emmanuel et al.)

SEM observations of Kraw(a), K7d (b) and K90d (c)

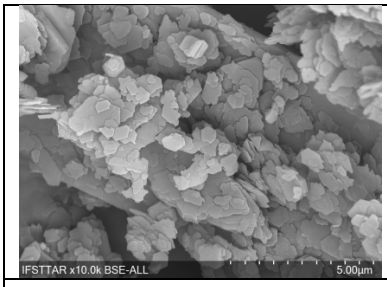

a)

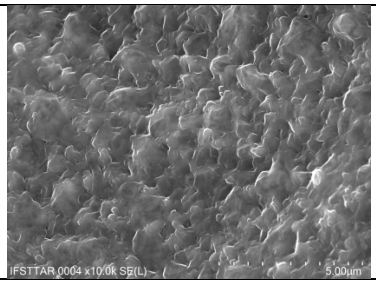

b)

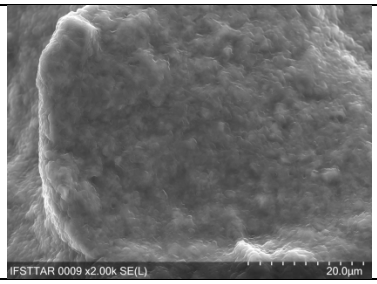

c)

Figure 4 (Emmanuel et al.)

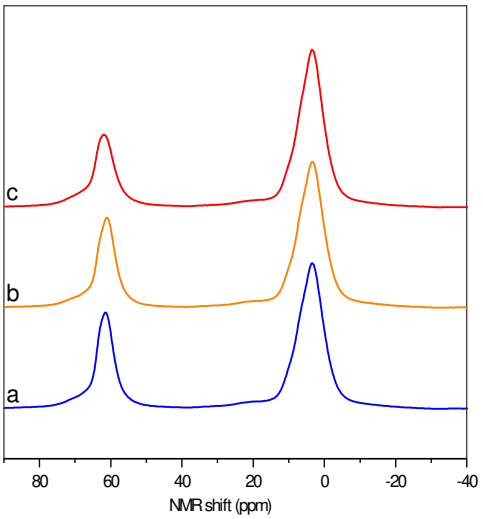

A- ^{27}Al MAS spectra of K5M1d (a), K5M3d (b) and K5M7d (c). Spectra are normalized to the same area.

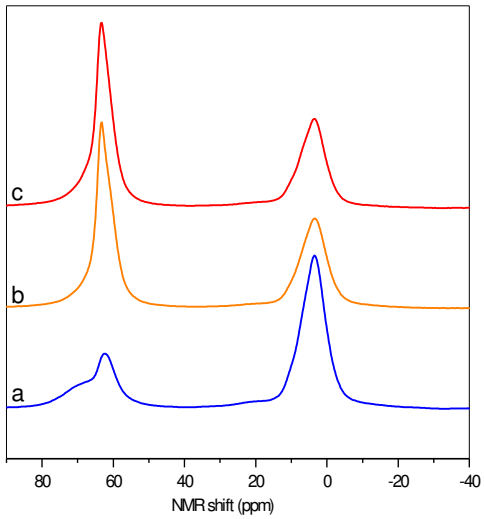

B- ^{27}Al MAS spectra of K10M1d (a), K10M3d (b) and K10M7d (c). Spectra are normalized to the same area.

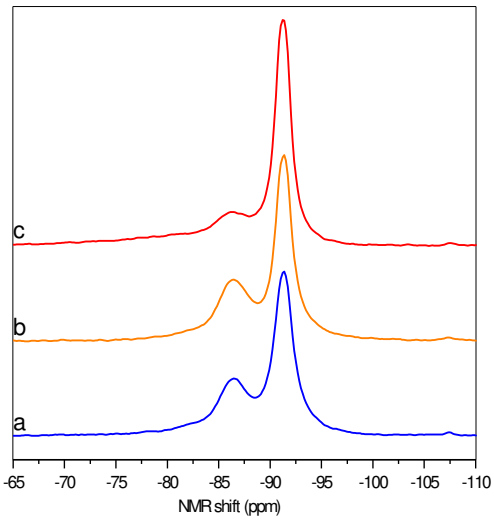

C- ^{29}Si MAS spectra of K5M1d (a), K5M3d (b) and K5M7d (c). MAS spectra are normalized to the same area.

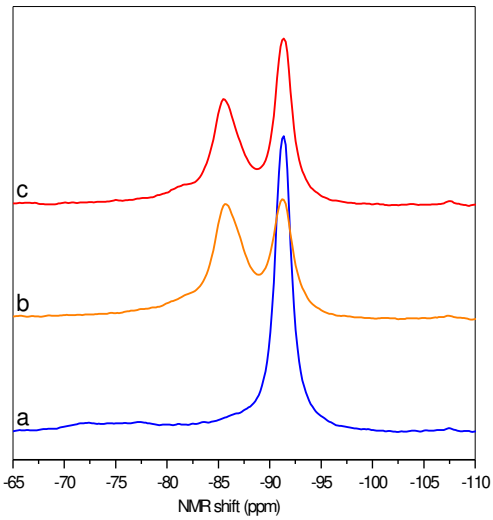

D- ^{29}Si MAS spectra of K10M1d (a), K10M3d (b) and K10M7d (c). MAS spectra are normalized to the same area.

Figure 5 (Emmanuel et al.)

SEM observations of K5M1d(a), K5M3d (b), K5M7d (c), K10M1d (d), K10M3d (e) and K10M7d (f). (HS:Hydrosodalite)

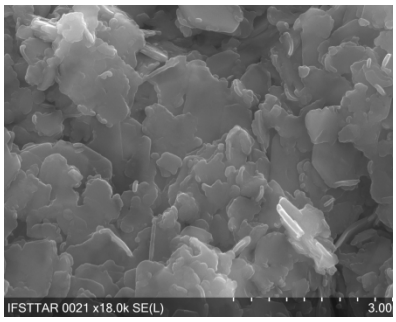

a) Kaolinite dissolution

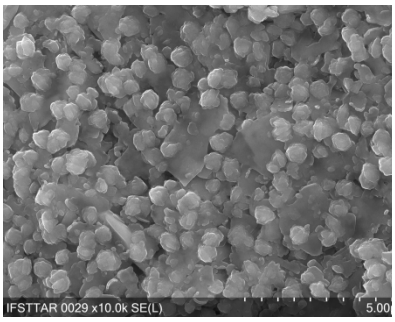

b) Gel + HS

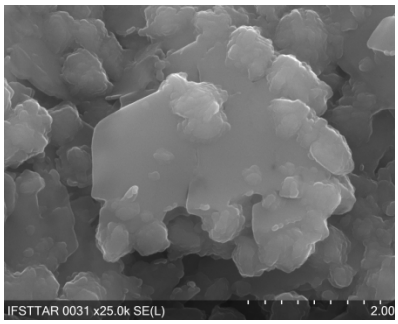

c) Gel + HS

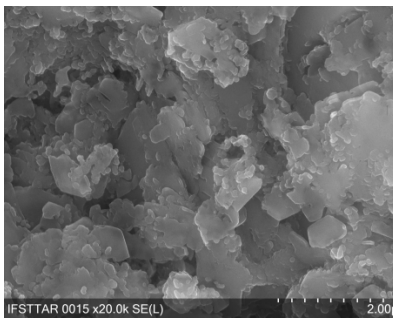

d) Kaolinite dissolution

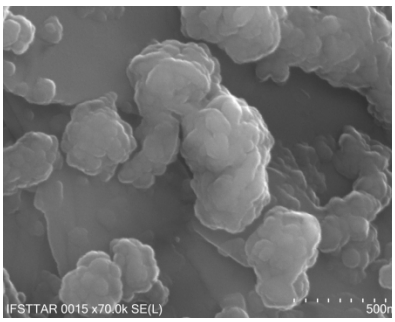

e) HS

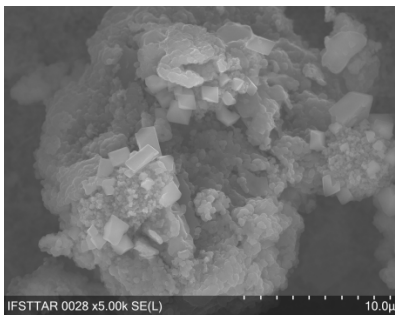

f) HS carbonation

Figure 6 (Emmanuel et al.)

SEM observations of K10M1d_90d (a), K10M7d_90d (b), K5M1d_90d (c) and K5M7d_90d (d). (HS:hydrosodalite)

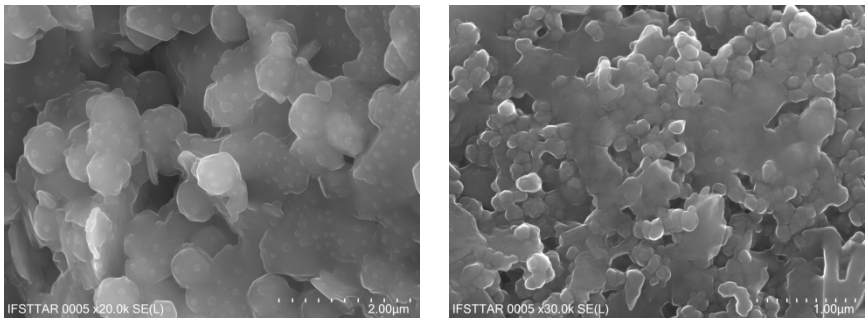

a) Gel + HS

b) Gel + HS

c) Gel + phase (Faujasite)

d) Gel + Phase (Phillipsite)

Figure 7 (Emmanuel et al.)

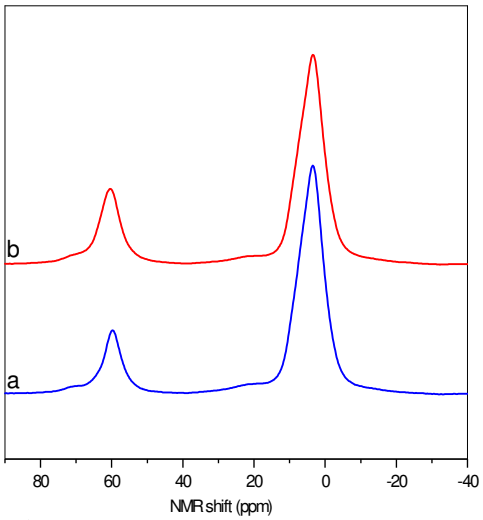

A-^{27}Al MAS spectra of K5M1d_90d (a) and K5M7d_90d (b). Spectra are normalized to the same area

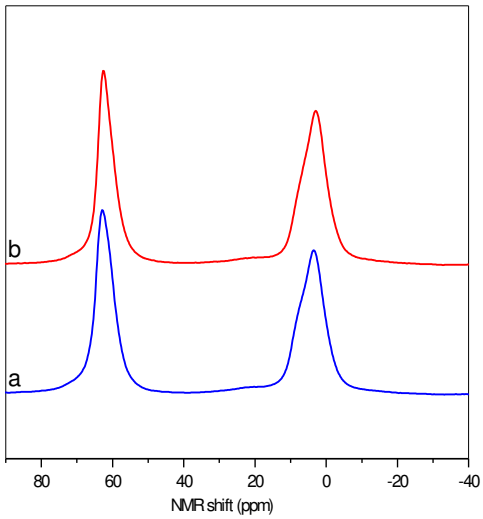

B-^{27}Al MAS spectra of K10M1d_90d (a) and K10M7d_90d (b). Spectra are normalized to the same area .

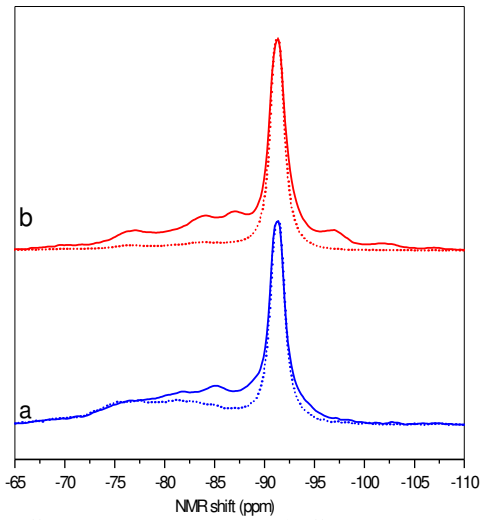

C- ^{29}Si MAS (straight lines) and ^{1}H-^{29}Si CP-MAS (dot lines) spectra of K5M1d_90d (a) and K5M7d_90d (b). MAS spectra are normalized to the same area. CP-MAS are normalized to the kaolinite signal (-91 ppm) used as an internal reference to highlight the difference of CP efficiency in the new phases formed.

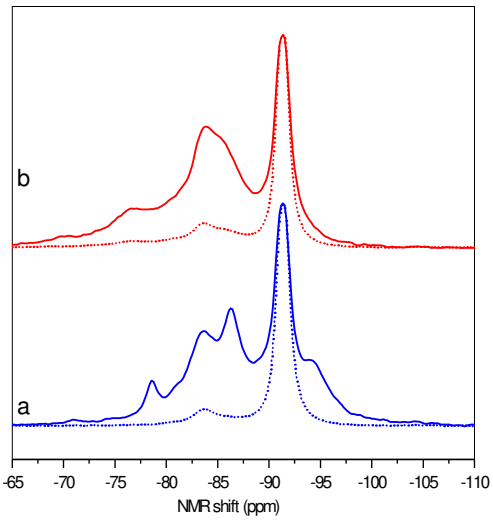

D- ^{29}Si MAS (straight lines) and ^{1}H-^{29}Si CP-MAS (dot lines) spectra of K10M1d_90d (a) and K10M7d_90d (b). MAS spectra are normalized to the same area. CP-MAS are normalized to the kaolinite signal (-91 ppm) used as an internal reference to highlight the difference of CP efficiency in the new phases formed.